Nanoscale

PAPER

View Article Online
View Journal | View Issue

Published on 18 May 2016. Downloaded by Shenzhen University on 21/09/2016 07:15:10.

Cite this: *Nanoscale*, 2016, **8**, 11234

Efficient plasma-enhanced method for layered $LiNi_{1/3}Co_{1/3}Mn_{1/3}O_2$ cathodes with sulfur atom-scale modification for superior-performance Li-ion batteries†

Qianqian Jiang,[a,b] Ning Chen,[b] Dongdong Liu,[b] Shuangyin Wang*[b] and Han Zhang*[a]

Received 29th March 2016,
Accepted 9th May 2016

DOI: 10.1039/c6nr02589g

www.rsc.org/nanoscale

In order to improve the electrochemical performance of $LiNi_{1/3}Co_{1/3}Mn_{1/3}O_2$ as a lithium insertion positive electrode material, atom-scale modification was realized to obtain the layered oxysulfide $LiNi_{1/3}Co_{1/3}Mn_{1/3}O_{2-x}S_x$ using a novel plasma-enhanced doping strategy. The structure and electrochemical performance of $LiNi_{1/3}Co_{1/3}Mn_{1/3}O_{2-x}S_x$ are investigated systematically, which confirms that the S doping can make the structure stable and benefit the electrochemical performance. The phys–chemical characterizations indicate that oxygen atoms in the initial $LiNi_{1/3}Co_{1/3}Mn_{1/3}O_2$ have been partially replaced by S atoms. It should be pointed out that the atom-scale modification does not significantly alter the intrinsic structure of the cathode. Compared to the pristine material, the $LiNi_{1/3}Co_{1/3}Mn_{1/3}O_{2-x}S_x$ shows a superior performance with a higher capacity (200.4 mA h g^{-1}) and a significantly improved cycling stability (maintaining 94.46% of its initial discharge capacity after 100 cycles). Moreover, it has an excellent rate performance especially at elevated performance, which is probably due to the faster Li^+ transportation after S doping into the layered structure. All the results show that the atom-scale modification with sulfur atoms on $LiNi_{1/3}Co_{1/3}Mn_{1/3}O_2$, which significantly improved the electrochemical performance, offers a novel anionic doping strategy to realize the atom-scale modification of electrode materials to improve their electrochemical performance.

Introduction

The lithium-ion battery has been considered to be the most promising alternative, environmentally friendly energy because of global warming and the exhaustion of fossil fuels.[1–4] Over the past decades, lithium-ion batteries have been applied as an essential electric source for portable electronic devices[5–7] due to their low cost, fast charge discharge reactions, high coulombic efficiency and non-toxicity. $LiCoO_2$ has been used as the major cathode material for lithium on secondary batteries since Sony first introduced $LiCoO_2$ as a cathode material. However, the relatively high cost and high toxicity of cobalt has led to the evaluation of other possible cathode materials. Among the lithium-ion secondary battery materials, manganese based layer-structured material $LiNi_{1/3}Co_{1/3}Mn_{1/3}O_2$, which possesses a good electrochemical performance and safety characteristics, is considered to be one of the most promising battery materials. This material attracts significant interest because the combination of nickel, manganese and cobalt can provide advantages such as a high reversible capacity with mild thermal stability at a charged state.[8,9] Therefore, there is a strong demand to improve their electrochemical performance to meet commercial demand. Recently, several research groups have investigated the substitution of lithium ions for transition metal ions,[10–13] the so-called overlithiation,[14–17] to improve electrochemical properties.[18–21] In this case, a decrease in the obtainable capacity is expected because the main redox reaction is ascribed to the $Ni^{2+/4+}$ and $Co^{3+/4+}$. The substitution for Mn sites in $LiNi_{1/3}Co_{1/3}Mn_{1/3}O_2$ may not decrease the capacity because Mn does not take part in the redox reaction in the voltage range between 2.7 and 4.8 V. However, the retention of the discharge capacity is not satisfactory. Meanwhile, Kubo *et al.*[22] and Naghash *et al.*[23,24] observed that the crystal structure of the material was stabilized by substituting O for $LiNiO_2$ with fluorine, resulting in the significant improvement of $LiNiO_2$ cycling performance during the intercalation/deintercalation process. Therefore,

[a]*SZU-NUS Collaborative Innovation Center for Optoelectronic Science & Technology, Key Laboratory of Optoelectronic Devices and Systems of Ministry of Education and Guangdong Province, College of Optoelectronic Engineering, Shenzhen University, Shenzhen 518060, China. E-mail: hzhang@szu.edu.cn*

[b]*State Key Laboratory of Chem/Bio-Sensing and Chemometrics, College of Chemistry and Chemical Engineering, Hunan University, Changsha, 410082, P. R. China. E-mail: shuangyinwang@hnu.edu.cn*

†Electronic supplementary information (ESI) available. See DOI: 10.1039/c6nr02589g

This journal is © The Royal Society of Chemistry 2016

Published on 18 May 2016. Downloaded by Shenzhen University on 21/09/2016 07:15:10.

anionic substitution may be another possible way to tune the electronic properties and electrochemical performance of cathode materials.[22,25] Heteroatom doping has been demonstrated to be an efficient strategy to modify the structure and electronic properties and thus the electrochemical performance. For example, previously, we reported systematically that heteroatom doping into graphene, carbon nanotubes and other two-dimensional materials could efficiently improve their electrochemical performance due to the modified electronic properties and the introduced defect sites.[26]

In this study, a novel simple plasma-enhanced method is used for atom-scale modification to dope sulfur atoms into the classical $LiNi_{1/3}Co_{1/3}Mn_{1/3}O_2$ cathode. The structure of the layered $LiNi_{1/3}Co_{1/3}Mn_{1/3}O_2$ and the possible structure of sulfur doped $LiNi_{1/3}Co_{1/3}Mn_{1/3}O_2$ ($LiNi_{1/3}Co_{1/3}Mn_{1/3}O_{2-x}S_x$) are shown in Scheme 1. During the plasma reaction, the applied RF power is only set at 200 W and the optimal reaction time is 20 min, so the energy consumption of this experiment only needs 2.4×10^5 J, which is less than the commercial reaction. In the conventional method, the power of the tube furnace is commonly set at 2.5 kW, and the reaction time is longer than 2 h, which leads to an energy consumption larger than the plasma technology. Therefore, it can reduce the cost of the reaction to a great extent. Furthermore, during the plasma reaction, the end gas can be dealt with in a conical flask, which is easier than that of the conventional method for a quite long reaction time. In addition, plasma as one of the four fundamental states of matter consists of charged particles and a set of neutral particles, in which the positive and negative ions are completely free showing a high chemical activity. Through the inelastic collision between each other, the activation state of the reactant ion is formed, which can relatively easily promote the chemical reaction. Due to the high efficiency of the plasma method, it can also reduce the danger to the environment. From the chemical viewpoint, in plasma, there exist a large number of ions, electrons, excited states of atoms, molecules and free radicals, which have high activity. The plasma method can use these highly reactive species to promote certain chemical reactions which can not react under normal conditions. At the same time, the parameters of the plasma equipment are very easy to control, which further indicates that the plasma technology has good application prospects for the large-scale synthesis of cathode materials for lithium-ion batteries. The most important is that the atom-scale modification can realize the modification on the materials. The sulfur anion doping could improve the electronic properties and thus enhance the electrochemical performance as cathode materials in Li-ion batteries. On the other hand, proper modification may lead to stabilized electrode materials for durable Li-ion batteries.

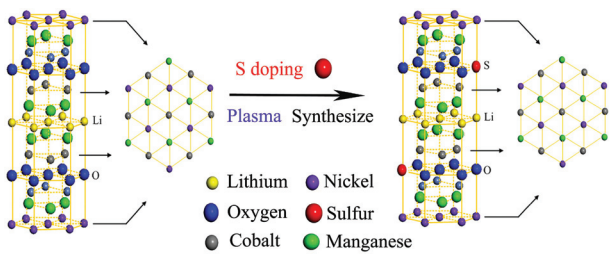

Scheme 1 Structures of the layered type $LiNi_{1/3}Co_{1/3}Mn_{1/3}O_2$ and $LiNi_{1/3}Co_{1/3}Mn_{1/3}O_{2-x}S_x$.

Experimental section

In order to make the uniform mixture, the $LiNi_{1/3}Co_{1/3}Mn_{1/3}O_2$ (denoted as LNCM) powder (supplied by Tianjiao Tech.) was mixed with a measured amount of thiourea at a molar ratio 10 : 1. Then the mixture was transferred into the plasma-enhanced tube furnace. The temperature of the tube furnace was set at 500 °C with a heating rate 10° min^{-1}. The plasma was introduced using an RF power supply at 13.56 MHz, and the applied RF power was set at 200 W. Argon was used as the shielding gas with a flow rate of 5 sccm and the total pressure of the chamber was kept under 50 Pa. The reaction time was controlled from 10 min to 30 min. The samples of $LiNi_{1/3}Co_{1/3}Mn_{1/3}O_{2-x}S_x$ synthesized using the plasma-enhanced method using thiourea as the sulfur source were defined as LNCM-S-*X* (*X* represents the plasma time: 10, 20, or 30 min).

Powder X-ray diffraction (XRD; Model D2500v/pc, Rigaku, Japan) measurements using Cu K radiation (40 kV, 200 mA) were carried out to characterize the structural properties of the synthesized compounds. XRD data were obtained 2θ = 10–80° with a step size of 0.02°. The as-prepared powders were observed using a scanning electron microscope (FEI Nova, NanoSEM 230). All XPS spectra were corrected on an ESCALAB 250Xi photoelectron spectrometer and curve fitting and background subtraction were accomplished.

The electrochemical characterization was performed using CR2032 coin-type cells. Cathodes for evaluating the electrochemical performance were prepared by mixing 80 wt% active materials with 10 wt% Super P carbon black and 10 wt% polyvinylidene fluoride in *N*-methylpyrrolidinone to create the electrode slurry. They were then dried in a vacuum oven at 120 °C for 12 h. The electrolyte used was a 1 M $LiPF_6$-ethylene carbonate (EC)/dimethyl carbonate (DMC) (1 : 1 by volume). The cell was assembled in an argon-filled dry box and tested at room temperature. The cyclic voltammetry (CV) and electrochemical impedance spectroscopy (EIS) of the cells were conducted on an AUT85794 with a frequency range from 100 kHz and 10 mHz. The CV was measured on an AUT85794 (made in the Netherlands) in a voltage range from 3.2 to 4.8 V with scan rate of 0.1 mV s^{-1}. The galvanostatic cycling tests of the assembled cells were carried out on a LAND CT2001A battery tester (Wuhan, China) in the voltage range of 2.8–4.3 V (*vs.* Li^+/Li).

Computational details

Our total energy and the binding energy were performed using the density functional theory as implemented in the Vienna

Published on 18 May 2016. Downloaded by Shenzhen University on 21/09/2016 07:15:10.

ab initio simulation package (VASP).[27,28] The exchange correlation energy and potential are described as GGA in the scheme of Perdew–Burke–Ernzerh of (PBE).[29] The 4 × 4 × 4 Monkhorst Pack *k*-points were used and in all calculations the plane wave energy cutoff was set at 400 eV to ensure that the energies were converged within 0.1 meV per atom. The pure LNCM structure was fully optimized including its lattice constant. For the geometry optimizations, all the internal coordinates were relaxed until the Hellmann–Feynman forces were less than 0.005 eV $Å^{-1}$. The crystal structures, total energy and binding energy values (E_b) of LNCM and LNCM-S are shown in Table S1.† The binding energy E_b is defined as: $E_b = E_{LNCM} + E_{atom} - E_{total}$, where E_{total} is the energy of the whole configuration, E_{LNCM} is the energy of the (relaxed) LNCM with a vacancy and E_{atom} represents the energy of an isolated dopant atom.

$$E_{LNCM\text{-}S} = E_{LNCM\text{-}S} - E_{LNCM} - E_S + E_O = 3.49 \text{ eV}.$$

After the DFT calculations, we can clearly find that the total energy of LNCM is a little lower than that of LNCM-S, which indicates that the LNCM-S possibly has the higher activity than LNCM. The binding energy of LNCM-S is about 3.49 eV, which indicates that the structure of LNCM-S is more stable than that of LNCM. It may be good for the lithium insertion/deinsertion during the charge and discharge process. Therefore, the material possibly has a better electrochemical performance than pristine LNCM. In order to further confirm that the S doping can make the structure stable and benefit the electrochemical performance, the binding energies of the lithium deinsertion during the charge process with the pristine LNCM and LNCM-S are calculated. From the calculation result, we can find that the binding energies of the lithium deinsertion for LNCM-S (4.36 eV) are larger than that for the pristine LNCM which indicates that the lithium deinsertion during the charge process with LNCM-S is easier than that of the pristine LNCM. In order to explore the electronic structure and transport properties of the S-doped LNCM, we performed DOS calculations (Fig. S1†). Since the layered lattice structure is well preserved after the sulfur doping, the linear energy dispersion near the Dirac point is not entirely destroyed. Effectively, the Fermi level (EF) of the LNCM-S system (4.78 eV) is a little higher than that of LNCM (4.73 eV), which indicates that the structure of LNCM becomes more stable due to the partial oxygen atom being replaced by the sulfur atom. Therefore, LNCM-S has an excellent electrochemical performance due to the S doping on the structure.

Results and discussion

As described in the Experimental section, thiourea is used as the S source to realize the atom-scale modifications to atomically dope S into the commercial LNCM cathode. The thiourea is initially evaporated and decomposed to NH_3 and H_2S[26] at the proper temperature to flow through the plasma-generator tube, which results in H_2S and NH_3 plasma reacting with the LNCM. Since the N in NH_3 is a positive ion, which is difficult to react with LNCM. Therefore, no N species are observed in the treated samples, as shown in the following XPS and EDS characterizations. The S anion plasma can efficiently react with the metal species to realize the atom-scale modification on LNCM. XRD of the undoped and doped $LiNi_{1/3}Co_{1/3}Mn_{1/3}O_2$ was carried out to determine the effect of the S doping on the crystal structure of $LiNi_{1/3}Co_{1/3}Mn_{1/3}O_2$ as shown in Fig. 1. The main intense diffraction peaks of the two samples can be indexed based on a hexagonal α-$NaFeO_2$ structure (space group: $R\bar{3}m$), which is consistent with $LiNi_{1/3}Co_{1/3}Mn_{1/3}O_2$ reported literatures.[12,13,16,17] At the same time, we find that there are no other reflection peaks observed in their XRD patterns which indicates that doping a small amount of sulfur into the material $LiNi_{1/3}Co_{1/3}Mn_{1/3}O_2$ did not generate any impurities in the final product or destroy the integral layered structure of the material. By comparing the two patterns, it can be seen that the splits in the (006)/(102) and (108)/(110) of LNCM-S-20 are more obvious than those of LNCM, which illustrates that LNCM-S-20 has a highly ordered layer structure, and the well-developed layered structure is probably achieved by the S partial substitution of O. In order to further confirm that the sulfur atom has been doped into the lattice, the lattice parameters of the LNCM and LNCM-S-20 powders obtained from the Rietveld refinements of the XRD patterns are shown in Table S2.† The refinement parameters and the refined XRD patterns of LNCM and LNCM-S-20 are shown in Fig. S2.† And the refined lattice parameters within the experimental errors of the two samples are identical to the reported results.[30,31] Compared to the lattice parameters of LNCM, we find that the parameters a and c are a little smaller than those of LNCM, which further confirms that the sulfur atom has been doped into the lattice.[32] At the same time, c/a of LNCM-S-20 are a little larger than those of LNCM, which indicates that the layer space of the material has increased due to the substitution of sulfur for oxygen. Considering that the small amount of S doping can make the structure more stable, it will be beneficial for the electrochemical performance of the material.

Comparing the morphology change of the cathode materials before and after the atom-scale modification is of

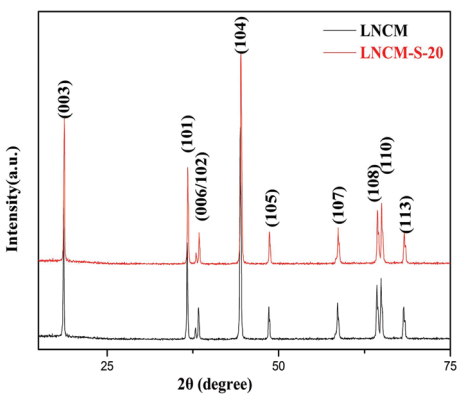

Fig. 1 X-ray diffraction patterns of the pristine LNCM-C and LNCM-S-20.

This journal is © The Royal Society of Chemistry 2016

Published on 18 May 2016. Downloaded by Shenzhen University on 21/09/2016 07:15:10.

great interest. The scanning electron microscopy (SEM) images of the pristine LNCM and doped LNCM-S-20 are investigated in Fig. 2 and S3.† It can be clearly observed that the two samples show a similar structure. In order to further study the changes on the surface of the sample, the SEM images with small scale bars are shown in Fig. 2. From the SEM images in Fig. 2, we can see that the two samples have a similar regular polygonal shape, indicating that the S surface doping did not significantly affect the microscopic morphology of the material. However, it can be seen from Fig. 2b that the surface of the doped LNCM-S-20 becomes much rougher than that of LNCM, possibly due to the plasma etching effect on the surface of the material. The changes on the surface may be good for the lithium insertion/deinsertion during the charge and discharge process. In the EDS image (see Fig. S4a†), the molar ratios of Mn, Ni and Co in the two samples are both close to 1 : 1 : 1, which is consistent with the ideal layer structure $Li[Ni_{1/3}Co_{1/3}Mn_{1/3}]O_2$. Besides, except S (the percentage of S is 1.32%), there is no other element signal in Fig. S4b,† which indicates there is no impurity existing in the product caused by S doping. The existence of S suggests that S has been doped into the material $LiNi_{1/3}Co_{1/3}Mn_{1/3}O_2$ and the content of S is very low, which indicates that the S only replaces a small part of the O in LNCM. In order to confirm the distribution of the S doping, SEM images with a wide range and the corresponding elemental mappings are collected. Fig. 3 shows the SEM images of LNCM-S-20 and the element-mapping images of each of the constituent elements (Ni, Mn, Co, O) and sulfur. It should be emphasized that the doped sulfur atoms are uniformly distributed on the electrodes. The results further confirm that the atom-scale modification with sulfur atoms is successfully realized using the novel efficient plasma-enhanced method.

In order to investigate the effect of the S doping on the electrochemical performance of the material, the electrochemical properties of LNCM and LNCM-S-20 are systematically investigated by studying their discharge capacity in the voltage range of 2.8–4.3 V at 0.2 C and the cycling stability. From Fig. 4a, we can see that the discharge curves of the two samples exhibit obvious discharge plateaus associated with the one-stage mechanism of the electrochemical lithium intercalation (at about 3.9 V),[8,10] which indicates the modification

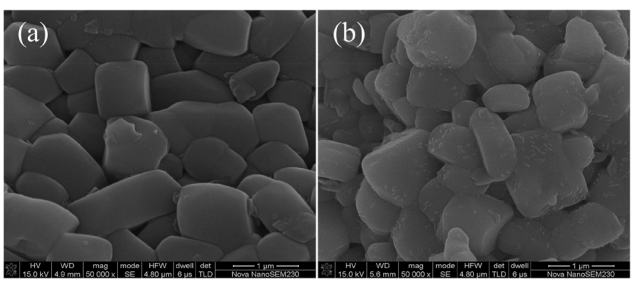

Fig. 2 Scanning electron microscopy images of (a) the pristine LNCM and (b) LNCM-S-20.

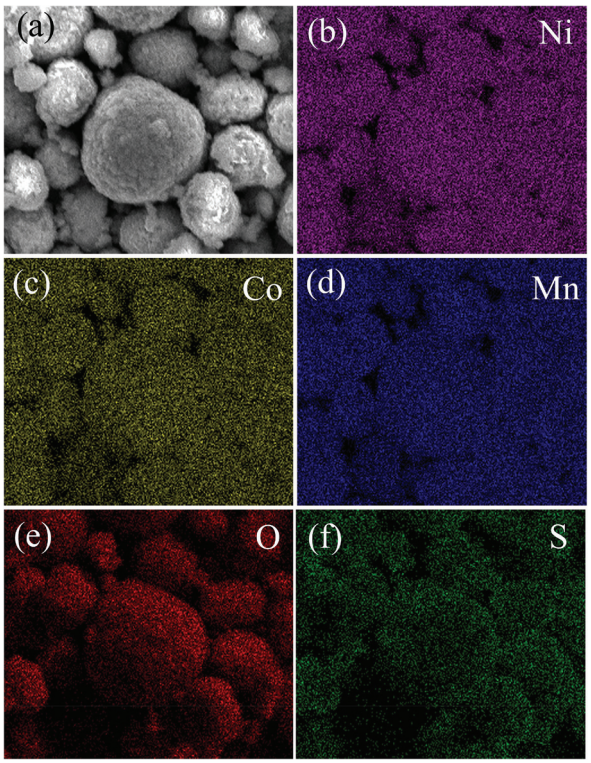

Fig. 3 (a) SEM image of the sample LNCM-S-20, corresponding elemental mappings of (b) Ni, (c) Co, (d) Mn, (e) O and (f) S.

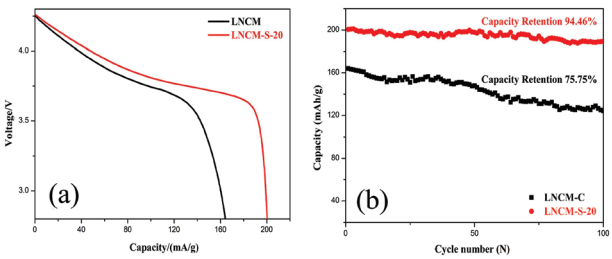

Fig. 4 Initial discharge curves (a) in the voltage range of 2.8–4.3 V and cycling stability curves (b) of commercial LNCM and modified LNCM-S-20.

by S doping did not alter the layered structure of $LiNi_{1/3}Co_{1/3}Mn_{1/3}O_2$. Obviously, the discharge platform of LNCM-S-20 is longer than that of LNCM, indicating a higher battery capacity. The discharge capacity of LNCM-S-20 is 200.4 mA h g^{-1}, which is much higher than that of LNCM (164.1 mA h g^{-1}). It is clear that the S doping has greatly improved the initial discharge capacity. At the same time, the discharge capacities of the modified LNCM with the different plasma times (seeing ESI Fig. S5a†) are all higher than that of commercial LNCM, which further illustrates the important role of S doping on improving the electrochemical performance of the material.

The discharge capacities as a function of their cycle numbers at 0.2 C between 2.8 and 4.3 V at the room tempera-

Published on 18 May 2016. Downloaded by Shenzhen University on 21/09/2016 07:15:10.

ture are shown in Fig. 4b. The cycling behavior of LNCM-S-20 is quite stable and displayed better capacity retention of 94.46% capacity retention after 100 cycles compared to the corresponding value of 75.69% for commercial LNCM. In other words, LNCM-S-20 exhibits a slower capacity fading on cycling with an average capacity loss of 0.111 mA h g^{-1} per cycle during 100 charge–discharge cycles than that of LNCM with an average capacity loss of 0.399 mA h g^{-1} per cycle. Better capacity retention means that the structural stability is improved by the sulfur anion doping. Meanwhile, the cycling performance of the samples with the different plasma times was investigated in Fig. S5b.† The capacity retention of PLA-LNCM-S-10, LNCM-S-20 and PLA-LNCM-S-30 are 85.60%, 94.46% and 85.60%, respectively, which is much higher than that of LNCM. It is believed that the doped S atoms can suppress the formation of Ni^{2+}, thereby preventing disruption of the ordering of the Li layer and improving the cycling performance of the material, which is much better than that of the existing literature (seeing the ESI Table S3†).

It is well known that rate capability can be affected strongly by the structure of a cathode material. The rate capabilities of LNCM-C and LNCM-S-20 ranged from 0.2 to 5 C rate are shown in Fig. 5a. Charge and discharge processing of the cells are cycled ten times at the same current densities in the range of 2.8–4.3 V at room temperature. Specific capacity of 200.6 mA h g^{-1} is obtained at the rate of 0.2 C for LNCM-S-20 and then decreased to 195.2 mA h g^{-1} at 0.5 C, 186.4 mA h g^{-1} at 1 C, finally, 175.8 mA h g^{-1} at 2 C, corresponding to the capacity retention of 98.87%, 97.80% and 96.19%, respectively. This rate capability is much higher than that for the pristine LNCM. The specific capacities of the pristine LNCM are only 160.7 mA h g^{-1}, 153.5 mA h g^{-1}, 137.2 mA h g^{-1} and 106.5 mA h g^{-1}, and their capacity fadings are 2.12%, 5.15%, 8.53%, and 7.79% at 0.2 C, 0.5 C, 1 C and 2C after 10 cycles, respectively, which indicates that the S doping plays an important role in the improvement of the rate capability. At the same time, we can find that after the different rate tests, the capacity retention of LNCM-S-20 back to 0.2 C is 99.55%, which is higher than that of LNCM. In addition, LNCM-S-20 shows excellent stability and no obvious degradation at each stage of the current rate, which indicates that S doping can effectively improve the cycling performances of the material. This excellent rate performance is probably due to atom-scale modification, which makes the layered structure more stable, and thus the rate of Li ion insertion/extraction into/out of the layered $LiNi_{1/3}Co_{1/3}Mn_{1/3}O_2$ structure is significantly improved.

In order to further confirm the effect of the S doping, the cycling performance of the material at elevated temperatures was also investigated, the cycling performances of the materials at 0.2 C between 2.8 and 4.5 V at 55 °C are shown in Fig. 5b. It is clearly found that the capacity of LNCM fades more quickly than that of LNCM-S-20.[33] The pure $LiNi_{1/3}Co_{1/3}Mn_{1/3}O_2$ exhibits a gradual capacity fading upon cycling, and the capacity retention is only 43.43% over 60 cycles. However, LNCM-S-20 maintains 72.75% of its initial capacity after 60 cycles, which shows a much better capacity retention than that of LNCM. With the S doping in $LiNi_{1/3}Co_{1/3}Mn_{1/3}O_2$, the thermal stability of the charged cathode material in the electrolyte is greatly improved. It is assumed that the partial substitution of oxygen with sulfur might create a more flexible structure in the S-doped layered $LiNi_{1/3}Co_{1/3}Mn_{1/3}O_2$ framework, which can increase the ion transport for lithium by the sulfur doping. When oxygen is substituted with sulfur, it suppresses the formation of Ni^{2+} and prevents the disruption of the ordering of the Li layer. The resulting lithium nickelate does not show restrained distortion, and therefore the cycle life is improved. The excellent elevated performance further confirms the benefit of S doping, which is also consistent with the other electrochemical performance tests.

In order to understand the effect of the S doping on layered $LiNi_{1/3}Co_{1/3}Mn_{1/3}O_2$ cathode materials, cyclic voltammetry tests are conducted on both the pristine and the S doped $LiNi_{1/3}Co_{1/3}Mn_{1/3}O_2$ cathode materials at 0.1 mV s^{-1} from 3.2 to 4.8 V. Fig. 6a displays the CV curves of LNCM and LNCM-S-20 with similar curves and there is no other peak appearing in the CV curve of LNCM-S-20. The anodic scan shows a sharp and intense peak centered at 3.95 V and a second low-intensity peak at 4.65 V corresponding to the platform in the charge curve. At the same time, an obvious cathodic peak is observed at about 3.6 V, consistent to the platform on the discharge curve, which indicates that there is no structural distortion caused by the multiphase reactions during the charging and discharging cycling process. The redox peaks are Ni^{2+}/Ni^{4+} couples corresponding to the lithium ion emergence from the anode materials and reduction on the cathode corresponding to Ni^{2+} oxidized to Ni^{4+}. At the same time, there is a

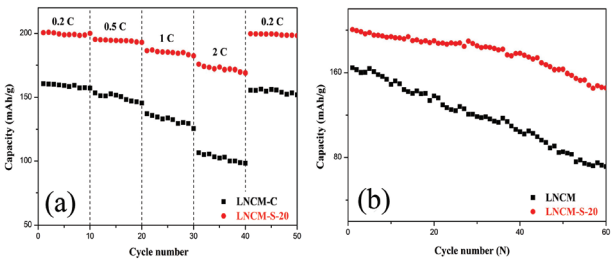

Fig. 5 (a) Rate capability tests and (b) cycling performances at 55 °C for LNCM and LNCM-S-20 in the voltage range 2.8–4.3 V Li/Li^+.

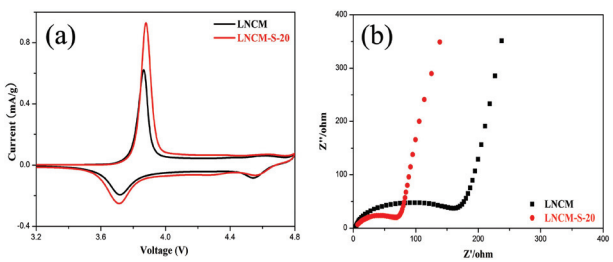

Fig. 6 (a) Cyclic voltammograms in the voltage range 3.2–4.8 V Li/Li^+ and (b) Nyquist plots of samples LNCM and LNCM-S-20.

This journal is © The Royal Society of Chemistry 2016

Published on 18 May 2016. Downloaded by Shenzhen University on 21/09/2016 07:15:10.

small peak at 4.5–4.6 V in both the cyclic voltammograms conclusively assigned to the Co^{3+}/Co^{4+} couple.[34,35] However, we can clearly see that the oxidation current peak in LNCM-S-20 is larger than that of LNCM, indicating the occurrence of lower polarization and the reversible oxidation reaction process at the cathode, which further illustrates that the S doped $Li(Ni_{1/3}Co_{1/3}Mn_{1/3})O_2$ synthesized using the plasma-enhanced method has a higher electronic conductivity than that of LNCM. Furthermore, the redox peak of LNCM-S-20 is also higher than that of LNCM, indicating that LNCM-S-20 has a better lithium intercalation/deintercalation and a faster electrode reaction than LNCM. The CV results demonstrate that the cathodic/anodic peak potentials are quite sensitive to the structure of the material, which can further demonstrate the important effect of S doping on the performance of material.

To further investigate the conductivity of the electrode materials with the S doping, electrochemical impedance spectroscopy (EIS) spectra are measured for the two materials before the charge/discharge test with two-electrode CR2032-type coin cells. It can be seen from Fig. 6b that all the EIS spectra consist of a high-frequency intercept, a broad semicircle and an inclined line, which can be fitted using the equivalent circuit model. The intercept in the high frequency region corresponds to the ohmic resistance (R_s), which combines resistance of the electrolyte and the contacts of the cell.[36–38] The diameters of the plots of the electrode provide the charge transfer resistance (R_{ct}) associated with the electrochemical process. In this work, the R_s values are almost the same throughout the experiments due to the same battery structure and fabrication technique. From the fitted results (see ESI Fig. S6†), we can see that LNCM-S-20 exhibits a smaller charge transfer resistance (R_{ct} = 73.2 Ω) than LNCM (R_{ct} = 170.8 Ω), due to the enhanced Li^+ transportation with the enlarged interlayer caused by the large S atom doping. The smaller R_{ct} favors the rapid electrochemical reactions and might improve the electrochemical performance of the active materials. This result is validated by the capacity and stability analyses discussed above.

In order to investigate the detailed information about the composition and electronic structure of LNCM-S-20, X-ray photoelectron spectroscopy (XPS) analysis is performed. As expected, Fig. 7a–c show the Co, Ni and Mn XPS core spectra for the two samples. In the two curves, we can find that a characteristic satellite peak around 860.3 eV is noted as the Ni $2p_{3/2}$ peak. Such a satellite peak is also observed in NiO, LiNiO and in Li(MnNi)O [39] and is explained as being due to the multiple splitting in the energy level of the Ni-containing oxides.[40] The Ni $2p_{3/2}$ spectrum gives two BE values. In the Co XPS spectra, the Co $2p_{3/2}$ spectra fits to a single peak with a BE of 779.5 eV, whose value match well with the BE reported for Co^{3+} in $LiCoO_2$.[35] At the same time, the binding energies for Mn $2p_{1/2}$ and Mn $2p_{3/2}$ measured from Fig. 7c are 653.79 eV and 642.09 eV, which closely match those values reported for $LiMn_2O_4$.[41] On the other hand, from Fig. 7, we can clearly see that peaks for Co 2p, Ni 2p and Mn 2p are shifted to a higher binding energy after the S doping. In order to easily to illustrate the phenomenon, Fig. S7† exhibits a scheme to illustrate why the Mn 2p core binding energy in $Li(Ni_{1/3}Co_{1/3}Mn_{1/3})O_2$ increases with the doping with S. It is the higher electron affinity of S compared with O that reinforces the Mn–O ionic bonds in the hexagonal α-$NaFeO_2$ structure (space group: $R\bar{3}m$) sites of $Li(Ni_{1/3}Co_{1/3}Mn_{1/3})O_2$, and hence the energy for emitting an electron from the Mn 2p core levels increases. Contrastingly, the Mn2p XPS core peaks of $LiMn_2O_{4-x}F_x$ decreased from 642.9 to 641.0 eV when the F content in $LiMn_2O_{4-x}F_x$ increased from 0 to 1.0.[42] Similarly, the high resolution S 2p peak can be fitted with two different peaks (Fig. 7d) in agreement with the previously reported S $2p_{3/2}$ and S $2p_{1/2}$,[43] indicating the formation of a bond between S and the transition metal. Due to the small amount of S substitution for O, there are some M–O (M = Co, Ni and Mn) replaced with M–S, which can increase the binding energy of elements in LNCM-S-20. Therefore, the structure is more stable and facilitates the lithium intercalation/deintercalation between the cathode and electrolyte. Thus, it is evident from the XRD and XPS results that the excellent cycling performance and rate capability of LNCM-S-20 in Fig. 4b and 5a are attributed to the improved structural stability from the S doping.

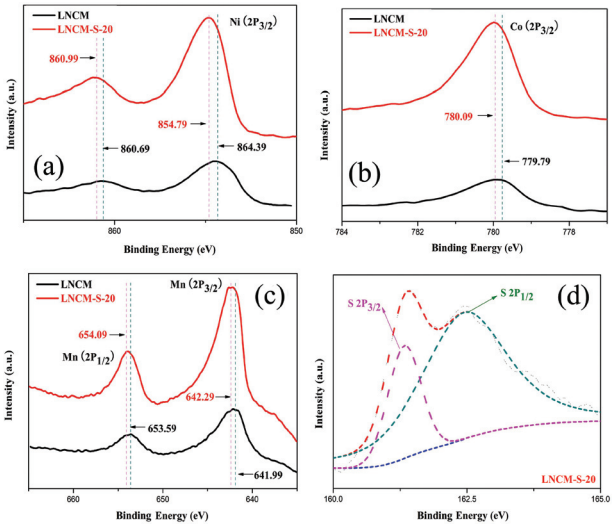

Fig. 7 XPS core level spectra of Co (a), Ni (b) and Mn (c) in LNCM and LNCM-S-20. The high resolution S 2p (d) XPS spectrum of LNCM-S-20.

Conclusion

In this study, we have successfully realized the atom-scale modification on $LiNi_{1/3}Co_{1/3}Mn_{1/3}O_2$ using plasma-enhanced sulfur doping. The surface modified $LiNi_{1/3}Co_{1/3}Mn_{1/3}O_2$ not only has a higher initial discharge (200.4 mA h g^{-1}) than that of the pristine sample (164.1 mA h g^{-1}), but also has an excellent cycling performance with only 5.54% capacity fading compared to 24.31% with the pristine one. More importantly, $LiNi_{1/3}Co_{1/3}Mn_{1/3}O_{2-x}S_x$ has a much better rate performance and elevated temperature properties than $LNi_{1/3}Co_{1/3}Mn_{1/3}O_2$,

Published on 18 May 2016. Downloaded by Shenzhen University on 21/09/2016 07:15:10.

due to the S doping with modified structural and electronic properties. The S doped LNCM shows a higher initial discharge capacity and a better cycling performance. Therefore, these interesting properties make this material an eco-friendly and highly efficient cathode material for lithium-ion batteries.

Acknowledgements

The work is supported by the National Natural Science Foundation of China (Grant No. 51402100, 21573066 and 61435010), the Youth 1000 Talent Program of China, and the Inter-discipline Research Program of Hunan University.

Notes and references

1 M. Armand and T. J.-M. Tarascon, *Nature*, 2008, **451**, 652.
2 L. Jungbae, K. Purushottam, L. Jinhyung, B. M. Moudgil and R. K. Singh, *J. Alloys Compd.*, 2013, **550**, 536.
3 T. F. Yi, Y. R. Zhu, X. D. Zhu, J. Shu, C. B. Yue and A. N. Zhou, *Ionics*, 2009, **15**, 779.
4 Q. Jiang, X. Wang, C. Miao and Z. Tang, *RSC Adv.*, 2013, **3**, 12088.
5 T. Yi, C. Yue, Y. Zhu, R. Zhu and X. Hu, *Rare Met. Mater. Eng.*, 2009, **38**, 1687.
6 Z. S. Zheng, Z. L. Tang, Z. T. Zhang and W. C. Shen, *J. Inorg. Mater.*, 2003, **18**, 257.
7 Q. Jiang, H. Zhang and S. Wang, *Green Chem.*, 2016, **18**, 662–666.
8 N. Yabuuchi and T. Ohzuku, *J. Power Sources*, 2003, **119**, 171.
9 Q. Jiang, L. Xu, J. Huo, H. Zhang and S. Wang, *RSC Adv.*, 2015, **5**, 75145.
10 T. Ohzuku and Y. Makimura, *Chem. Lett.*, 2001, **30**, 642.
11 K. M. Shaju, G. V. Subba Rao and B. V. R. Chowdari, *Electrochim. Acta*, 2002, **48**, 145.
12 D. C. Li, T. Muta, L. Q. Zhang, M. Yoshio and H. Noguchi, *J. Power Sources*, 2004, **132**, 150.
13 H. Ren, Y. Wang, D. Li, L. Ren, Z. Peng and Y. Zhou, *J. Power Sources*, 2008, **178**, 439.
14 J. M. Kim and H. T. Chung, *Electrochim. Acta*, 2004, **49**, 3573.
15 A. V. D. Ven and G. Ceder, *Electrochem. Commun.*, 2004, **6**, 1045.
16 L. S. Cahill, S.-C. Yin, A. Samoson, I. Heinmaa, L. F. Nazar and G. R. Goward, *Chem. Mater.*, 2005, **17**, 6560.
17 Y. W. Tsai, B. J. Hwang, G. Ceder, H. S. Sheu, D. G. Liu and J. F. Lee, *Chem. Mater.*, 2005, **17**(12), 3191–3199.
18 S. T. Myung, S. Komaba, K. Kurihara, K. Hosoya, N. Kumagai, Y. K. Sun, I. Nakai, M. Yonemura and T. Kamiyama, *Cheminform*, 2006, **37**, 1658.
19 Y. M. Todorov and K. Numata, *Electrochim. Acta*, 2004, **50**, 495.
20 H. C. Sun, O. A. Shlyakhtin, J. Kim and Y. S. Yoon, *J. Power Sources*, 2005, **140**, 355.
21 N. Tran, L. Croguennec, C. Labrugère, C. Jordy, P. Biensan and C. Delmas, *J. Electrochem. Soc.*, 2006, **153**, A261–A274.
22 K. Kubo, M. Fujiwara, S. Yamada, S. Arai and M. Kanda, *J. Power Sources*, 1997, **68**, 553.
23 A. R. Naghash and J. Y. Lee, *Electrochim. Acta*, 2001, **46**, 2293.
24 A. R. Naghash and J. Y. Lee, *Electrochim. Acta*, 2001, **46**, 941.
25 G. H. Kim, J. H. Kim, S. T. Myung, C. S. Yoon and Y. K. Sun, *J. Electrochem. Soc.*, 2005, **152**, A1707–A1713.
26 W. Xin, W. Jie, W. Deli, D. Shuo, M. Zhaoling, W. Jianghong, T. Li, S. Anli, O. Canbin and L. Qiuhong, *Chem. Commun.*, 2014, **50**, 4839.
27 G. Kresse and D. Joubert, *Phys. Rev. B: Condens. Matter*, 1999, **59**, 1758.
28 W. Kohn and L. J. Sham, *Phys. Rev.*, 1965, **140**, A1133.
29 J. P. Perdew, K. Burke and M. Ernzerhof, *Phys. Rev. Lett.*, 1996, **77**, 3865.
30 N. Yabuuchi and T. Ohzuku, *J. Power Sources*, 2003, **119**, 171.
31 D.-C. Li, T. Muta, L.-Q. Zhang, M. Yoshio and H. Noguchi, *J. Power Sources*, 2004, **132**, 150.
32 G. H. Kim, M. H. Kim, S. T. Myung and K. S. Yang, *J. Power Sources*, 2005, **146**, 602.
33 H. Li, Z. Wang, L. Chen and X. Huang, *Adv. Mater.*, 2009, **21**, 4593.
34 K. M. Shaju, G. V. S. Rao and B. V. R. Chowdari, *J. Electrochem. Soc.*, 2002, **150**, A1.
35 S. Madhavi, G. V. S. Rao, B. V. R. Chowdari and S. F. Y. Li, *J. Electrochem. Soc.*, 2001, **148**, A1279.
36 M. D. Levi, G. Salitra, B. Markovsky, H. Teller, D. Aurbach, U. Heider and L. Heider, *J. Electrochem. Soc.*, 1998, **146**, 1279.
37 K. A. Striebel, E. Sakai and E. J. Cairns, *J. Electrochem. Soc.*, 2001, **149**, 1–16.
38 K. A. Walz, C. S. Johnson, J. Genthe, L. C. Stoiber, W. A. Zeltner, M. A. Anderson and M. M. Thackeray, *J. Power Sources*, 2010, **195**, 4943.
39 A. F. Carley, S. D. Jackson, J. N. O'Shea and M. W. Roberts, *Surf. Sci.*, 1999, **440**, L868.
40 K. Amine, H. Tukamoto, H. Yasuda and Y. Fujita, *J. Electrochem. Soc.*, 1996, **143**, 1607.
41 K. M. Shaju, G. V. S. Rao and B. V. R. Chowdari, *Solid State Ionics*, 2002, **148**, 343.
42 J. T. Son and H. G. Kim, *J. Power Sources*, 2005, **147**, 220.
43 S. Yang, L. Zhi, K. Tang, X. Feng, J. Maier and K. Müllen, *Adv. Funct. Mater.*, 2012, **22**, 3634.

 This journal is © The Royal Society of Chemistry 2016